2026 American Control Conference (ACC)
May 27-29, 2026. New Orleans, Louisiana, USA

Electrochemical Fault Diagnosis for Lithium-Ion Batteries: Part 1 – Electrochemical Fault Modeling

Sara Sepasiahooyi and Shu-Xia Tang

Abstract— **Electrochemical faults arising from internal degradation-related side reactions in lithium-ion batteries play a crucial role in battery safety and performance. Accurate modeling and thorough understanding of these processes are essential. The side reactions considered in this study are two of the most critical degradation-related electrochemical mechanisms: Solid Electrolyte Interphase (SEI) film growth and lithium plating. The Doyle–Fuller–Newman model with Side Reactions (DFN+SR) and the Single Particle Model with electrolyte dynamics integrated with Side Reactions (SPMe+SR) are first described. Subsequently, reformulated models providing a parameterized representation of side-reaction dynamics suitable for diagnostic analysis are proposed. These models are developed with strong physical justification while offering substantially lower computational cost and complexity. The study is structured in two parts, each standing independently, and Part 2 complements Part 1 by developing fault diagnosis schemes. The proposed reformulated side-reaction models are simulated on a $LiFePO_4$ cell to capture the characteristic degradation behavior.**

Index Terms— **Lithium-ion battery; Fault modeling; Degradation; SEI film growth; Lithium plating.**

I. Introduction

Degradation in lithium-ion batteries arises from various electrochemical mechanisms, often triggered by high charge/discharge rates and extreme temperatures [1]. The primary degradation mechanisms include SEI film growth, lithium plating, structural changes, decomposition, and particle fracture [2]. This study focuses on the two critical mechanisms, SEI film growth and lithium plating. Mathematical models play a crucial role in analyzing, forecasting, and ultimately mitigating battery degradation through advanced control strategies. However, their high computational cost limits their applicability in many real-world scenarios, particularly when extensive simulations are required for tasks such as battery design or control. This highlights the demand for reformulated models that are both efficient and sufficiently accurate to capture degradation phenomena [3].

This study first presents the DFN model augmented with Side Reactions (DFN+SR), followed by the reduced-order Single Particle Model with electrolyte dynamics and Side Reactions (SPMe+SR). Building on these models, reformulated side reaction models are then developed with strong physical justification, explicitly grounded in fundamental electrochemical principles. These reformulated models provide a balanced compromise between accurately capturing degradation dynamics and maintaining computational efficiency. Furthermore, the reformulated side reaction models will be employed in Part 2 to develop an electrochemical fault diagnosis scheme. The main contributions of this work are as follows:

- This study employs the reduced model for SEI film growth first introduced by the authors in [4], and in this study its theoretical foundation is further strengthened with physical and mathematical justification. This model achieves a balance between capturing essential degradation behavior and reducing computational complexity, compared to the model in [3].
- In this study, a novel distributed model for lithium plating is developed to capture the nature of this degradation mechanism. The model captures both temporal dynamics and spatial distribution of lithium plating on the negative electrode surface. To the best of our knowledge, this is the first time a reformulated model for lithium plating, developed on rigorous mathematical and physical justification, is proposed, offering a balanced trade-off between physical fidelity and computational efficiency compared to the model in [3].
- Building on the recently proposed SR model in [3], this work reformulates the side-reaction dynamics as electrochemical fault terms suitable for diagnostic analysis. To the best of our knowledge, this is the first work that uses these models as a foundation for fault diagnosis frameworks.

In the rest of this paper, Section II presents the battery model. Section III introduces the models of side reaction mechanisms. Section IV shows the simulation results. Finally, Section V provides the conclusion and future work.

II. Battery model

In this section, the battery model DFN+SR is first presented, followed by the SPMe+SR model.

A. DFN+SR Model

The DFN model, a comprehensive mathematical framework, considers variations along the horizontal x-axis to capture the dynamic behavior, while variations along the vertical y-axis and depth z-axis are assumed negligible [5]. Degradation mechanisms, including SEI film growth and lithium plating, are incorporated into the DFN model [3], as illustrated in Fig. 1. Here, t denotes time, $r \in (0, R_s^{\pm})$ is the radial coordinate within a particle, and $x \in (0^j, L^j),\ j \in \{-, \text{sep}, +\}$ represents the spatial coordinate. The input and output of the system are the applied current $I(t)$ and the

S. Sepasiahooyi and S.-X. Tang (Corresponding author) are with the Department of Mechanical and Aerospace Engineering, Texas Tech University, Lubbock, TX, USA. ssepasia@ttu.edu, shuxia.tang@ttu.edu.

Authorized licensed use limited to: Texas Tech University. Downloaded on September 03,2026 at 21:39:47 UTC from IEEE Xplore. Restrictions apply.

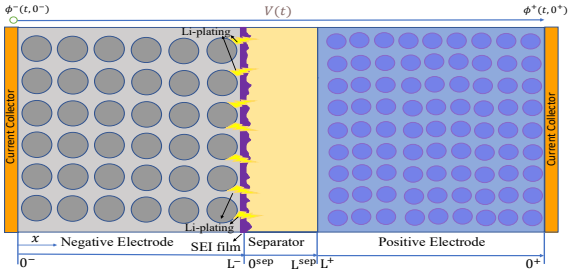

Fig. 1: DFN+SR schematic

terminal voltage $V(t)$, respectively. The equation for the solid-phase lithium concentration $c_{\mathrm{s}}^{\pm}(t,x,r)$ is described as:

$$\frac{\partial c_{\mathrm{s}}^{\pm}}{\partial t}(t,x,r)=\frac{1}{r^2}\frac{\partial}{\partial r}\left[D_{\mathrm{s}}^{\pm}r^2\frac{\partial c_{\mathrm{s}}^{\pm}}{\partial r}(t,x,r)\right], \quad (1)$$

The electrolyte-phase lithium concentration is given by:

$$\frac{\partial c_{\mathrm{e}}^{j}}{\partial t}(t,x)=\frac{\partial}{\partial x}\left[\frac{D_{\mathrm{e}}^{j,\mathrm{eff}}\left(c_{\mathrm{e}}^{j}(t,x)\right)}{\varepsilon_{\mathrm{e}}^{j}}\frac{\partial c_{\mathrm{e}}^{j}}{\partial x}(t,x)\right] + \frac{(1-t_c^0)\,a_{\mathrm{s}}^{j}}{\varepsilon_{\mathrm{e}}^{j}}\,j_n^{j}(t,x), j\in\{-,\mathrm{sep},+\}, \quad (2)$$

where the molar ion flux in different parts of the cell is [3]:

$$j_n^{-}(t,x)=j_{n,\mathrm{int}}^{-}(t,x)+j_{\mathrm{SR}}^{-}(t,x), \quad x\in\left(0^-,L^-\right), \quad (3)$$
$$j_n^{\mathrm{sep}}(t,x)=0, \quad x\in\left(0^{\mathrm{sep}},L^{\mathrm{sep}}\right), \quad (4)$$
$$j_n^{+}(t,x)=j_{n,\mathrm{int}}^{+}(t,x), \quad x\in\left(L^+,0^+\right), \quad (5)$$

where $j_{\mathrm{n,int}}^{-}(t,x)$ denotes the intercalation molar ion flux, and the side-reaction molar ion flux is defined as $j_{\mathrm{SR}}^{-}(t,x)=j_{\mathrm{SEI}}^{-}(t,x)+j_{\mathrm{pl}}^{-}(t,x)$. Their expressions are provided later. The equations for the solid-phase electric potential $\phi_{\mathrm{s}}^{\pm}(t,x)$, the electrolyte-phase electric potential $\phi_{\mathrm{e}}(t,x)$, the ionic current $i_{\mathrm{e}}^{\pm}(t,x)$, the molar ion flux $j_n^{\pm}(t,x)$, the exchange current density $i_0^{\pm}(t,x)$, and the overpotential $\eta^{\pm}(t,x)$ are described as:

$$\frac{\partial\phi_{\mathrm{s}}^{\pm}}{\partial x}(t,x)=\frac{i_{\mathrm{e}}^{\pm}(t,x)-I(t)}{\sigma^{\pm,\mathrm{eff}}}, x\in\left(0^{\pm},L^{\pm}\right), \quad (6)$$

$$\frac{\partial\phi_{\mathrm{e}}}{\partial x}(t,x)=\frac{-i_{\mathrm{e}}^{\pm}(t,x)}{\kappa_{\mathrm{e}}^{\pm,\mathrm{eff}}\left(c_{\mathrm{e}}^{\pm}(t,x)\right)}+\frac{2\mathrm{RT}}{F}\left(1-t_c^0\right) \times\left(1+\frac{d\ln f_{c/a}(t,x)}{d\ln c_{\mathrm{e}}^{\pm}(t,x)}\right)\frac{\partial\ln c_{\mathrm{e}}^{\pm}}{\partial x}(t,x), x\in\left(0^-,0^+\right), \quad (7)$$

$$\frac{\partial i_{\mathrm{e}}^{\pm}}{\partial x}(t,x)=a_{\mathrm{s}}^{\pm}Fj_n^{\pm}(t,x), x\in\left(0^{\pm},L^{\pm}\right), \quad (8)$$

$$j_n^{\pm}(t,x)=\frac{1}{F}i_0^{\pm}(t,x)\left[e^{\frac{\alpha_a F}{\mathrm{RT}}\eta^{\pm}(t,x)}-e^{-\frac{\alpha_c F}{\mathrm{RT}}\eta^{\pm}(t,x)}\right], \quad (9)$$
$$x\in\left(0^{\pm},L^{\pm}\right), \quad (10)$$

$$i_0^{\pm}(t,x)=k^{\pm}\left[c_{\mathrm{s}}^{\pm}(t,x,R_{\mathrm{s}}^{\pm})\right]^{\alpha_c}\times \left[c_{\mathrm{e}}^{\pm}(t,x)\left(c_{\mathrm{s,max}}^{\pm}-c_{\mathrm{s}}^{\pm}(t,x,R_{\mathrm{s}}^{\pm})\right)\right]^{\alpha_a}, x\in\left(0^{\pm},L^{\pm}\right), \quad (11)$$

$$\eta^{\pm}(t,x)=\phi_{\mathrm{s}}^{\pm}(t,x)-\phi_{\mathrm{e}}^{\pm}(t,x)-U^{\pm}\left(c_{\mathrm{s}}^{\pm}(t,x,R_{\mathrm{s}})\right) - FR_f^{\pm}(t)j_n^{\pm}(t,x), x\in\left(0^{\pm},L^{\pm}\right), \quad (12)$$

where $\varepsilon_{\mathrm{s}}^{\pm}$ and $\varepsilon_{\mathrm{e}}^{j}$ denote the volume fractions of the solid and electrolyte phases, respectively. F is the Faraday constant, and $k^{\pm}$ is the kinetic reaction constant. $D_{\mathrm{s}}^{\pm}$ represents the solid-phase diffusion coefficient. $\sigma^{\pm,\mathrm{eff}}$ denotes the effective conductivity of the solid phase. $R_f^{\pm}(t)$ is the SEI film resistance, and $U^{\pm}(.)$ is the open-circuit potential of the solid material. The effective electrolyte diffusivity is defined as $D_{\mathrm{e}}^{j,\mathrm{eff}}(c_{\mathrm{e}}^{j}(t,x))=D_{\mathrm{e}}^{j}(c_{\mathrm{e}}^{j}(t,x))\cdot(\varepsilon_{\mathrm{e}}^{j})^{\mathrm{brug}}$, and the effective electrolyte conductivity is $\kappa_{\mathrm{e}}^{j,\mathrm{eff}}(c_{\mathrm{e}}^{j}(t,x))=\kappa_{\mathrm{e}}^{j}(c_{\mathrm{e}}^{j}(t,x))\cdot(\varepsilon_{\mathrm{e}}^{j})^{\mathrm{brug}}$. The specific interfacial area of the electrodes is given by $a_s^{\pm}=\frac{3\varepsilon_s^{\pm}}{R_s^{\pm}}$.

In this study, the electrochemical side reaction in the battery model, expressed by its molar flux $j_{\mathrm{SR}}^{-}(t,x)$, is composed of SEI film growth molar flux $j_{\mathrm{SEI}}^{-}(t,x)$ and lithium plating molar flux $j_{\mathrm{pl}}^{-}(t,x)$. The side reaction models are explained as follows. The SEI layer forms on the surface of the electrode due to the reduction of electrolyte components during the charging cycles [1]. The SEI film growth consumes active lithium ions from the electrolyte and contributes to capacity loss. The SEI film growth is incorporated into the battery model via its current density $j_{\mathrm{SEI}}^{-}(t,x)$, modeled as [3]:

$$j_{\mathrm{SEI}}^{-}(t,x)=-\frac{1}{F}i_{0,\mathrm{SEI}}^{-}\exp\big(-\alpha_{\mathrm{SEI}}\tfrac{F}{RT}(\phi_{\mathrm{s}}^{-}(t,x) - \phi_{\mathrm{e}}(t,x)-U_{\mathrm{SEI}}^{-}(t)-\tfrac{R_f^{-}(t)}{a_{\mathrm{s}}^{-}L^{-}}I(t))\big), \quad (13)$$

where $i_{0,\mathrm{SEI}}^{-}$, $\alpha_{\mathrm{SEI}}^{-}$, and $U_{\mathrm{SEI}}^{-}(t)$ are SEI current density, SEI transfer coefficient, and SEI open-circuit potential, respectively. Lithium plating occurs when lithium ions are reduced to metallic lithium on the negative electrode surface instead of intercalating, typically under high charging rates, low temperatures, or near-full lithiation [6]. Lithium plating is modeled through its current density $j_{\mathrm{pl}}^{-}(t,x)$ as [3]:

$$j_{\mathrm{pl}}^{-}(t,x)=-\frac{1}{F}i_{0,\mathrm{pl}}^{-}\exp\big(-\alpha_{\mathrm{pl}}\tfrac{F}{RT}(\phi_{\mathrm{s}}^{-}(t,x)-\phi_{\mathrm{e}}(t,x) - U_{\mathrm{pl}}^{-}(t)-\tfrac{R_f^{-}(t)}{a_{\mathrm{s}}^{-}L^{-}}I(t))\big), x\in\left(0^-,L^-\right), \quad (14)$$

where $i_{0,\mathrm{pl}}^{-}$ and α_{pl}^{-} are the lithium plating current density and the lithium plating transfer coefficient, respectively. $U_{\mathrm{pl}}^{-}(t)$ is lithium plating open-circuit potential.

Remark 1. *Due to the greater impact of SEI film growth on the negative electrode than the positive electrode [7] and the fact that lithium plating occurs only on the negative electrode [8], this study focuses on side-reaction-related fault modeling for the negative electrode.*

The boundary conditions for $c_{\mathrm{s}}^{\pm}(t,x,r)$ in (1) are:

$$\frac{\partial c_s^{\pm}}{\partial r}(t,x,0)=0, x\in\left(0^{\pm},L^{\pm}\right), \quad (15)$$
$$\frac{\partial c_s^{\pm}}{\partial r}(t,x,R_s^{\pm})=\frac{-1}{D_s^{\pm}}j_n^{\pm}(t,x), x\in\left(0^{\pm},L^{\pm}\right). \quad (16)$$

The boundary conditions for (2), (7), and (8) are not provided

Authorized licensed use limited to: Texas Tech University. Downloaded on September 03,2026 at 21:39:47 UTC from IEEE Xplore. Restrictions apply.

in [3] but are extracted from [9] and given by:

$$\frac{\partial c_{\mathrm{e}}^{-}}{\partial x}(t,0^{-}) = \frac{\partial c_{\mathrm{e}}^{+}}{\partial x}(t,0^{+}) = 0, \tag{17}$$

$$D_{\mathrm{e}}^{-,\mathrm{eff}}(c_{\mathrm{e}}^{-}(t,L^{-}))\frac{\partial c_{\mathrm{e}}^{-}}{\partial x}(t,L^{-}) = D_{\mathrm{e}}^{\mathrm{sep,eff}}(c_{\mathrm{e}}^{\mathrm{sep}}(t,0^{sep})) \times \frac{\partial c_{\mathrm{e}}^{\mathrm{sep}}}{\partial x}(t,0^{\mathrm{sep}}), \tag{18}$$

$$D_{\mathrm{e}}^{\mathrm{sep,eff}}(c_{\mathrm{e}}^{\mathrm{sep}}(t,L^{\mathrm{sep}}))\frac{\partial c_{\mathrm{e}}^{\mathrm{sep}}}{\partial x}(t,L^{\mathrm{sep}}) = D_{\mathrm{e}}^{+,\mathrm{eff}}(c_{\mathrm{e}}^{+}(t,L^{+})) \times \frac{\partial c_{\mathrm{e}}^{+}}{\partial x}(t,L^{+}), \tag{19}$$

$$c_{\mathrm{e}}^{-}(t,L^{-}) = c_{\mathrm{e}}^{\mathrm{sep}}(t,0^{\mathrm{sep}}), \tag{20}$$

$$c_{\mathrm{e}}^{\mathrm{sep}}(t,L^{\mathrm{sep}}) = c_{\mathrm{e}}^{+}(t,L^{+}). \tag{21}$$

The boundary conditions for electrolyte potential (7) are:

$$\phi_{\mathrm{e}}(t,0^{-}) = 0, \tag{22}$$

$$\phi_{\mathrm{e}}(t,L^{-}) = \phi_{\mathrm{e}}(t,0^{\mathrm{sep}}), \tag{23}$$

$$\phi_{\mathrm{e}}(t,0^{\mathrm{sep}}) = \phi_{\mathrm{e}}(t,L^{+}). \tag{24}$$

The boundary conditions for ionic current (8) are:

$$i_{\mathrm{e}}^{-}\left(t,0^{-}\right) = i_{\mathrm{e}}^{+}\left(t,0^{+}\right) = 0, \tag{25}$$

$$i_{\mathrm{e}}^{-}\left(t,L^{-}\right) = i_{\mathrm{e}}^{+}\left(t,L^{+}\right) = I(t), \tag{26}$$

$$i_{\mathrm{e}}(t,x) = I(t) \text{ for } x \in [0^{\mathrm{sep}}, L^{\mathrm{sep}}]. \tag{27}$$

B. SPMe+SR model

In SPMe+SR, which is a reduced model of DFN+SR, each electrode is assumed to be idealized as a single spherical particle illustrated in Fig. 2. In this model, all particles

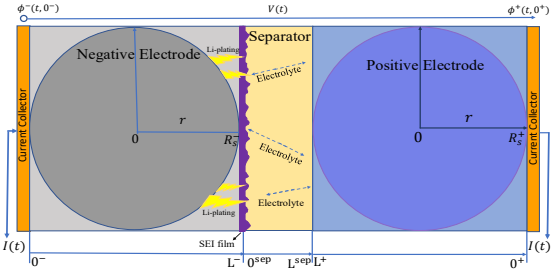

Fig. 2: SPMe+SR schematic

within each solid phase are assumed to behave identically. Consequently, $c_{\mathrm{s}}(t,x,r)$ and $j_n^{\pm}(t,x)$ are approximated as independent of the spatial coordinate, i.e., $c_{\mathrm{s}}(t,r)$ and $j_n^{\pm}(t)$. The solid-phase lithium concentration dynamics for the SPMe are given as follows [3]:

$$\frac{\partial c_{\mathrm{s}}^{\pm}}{\partial t}(t,r) = \frac{1}{r^2}\frac{\partial}{\partial r}\left[D_{\mathrm{s}}^{\pm} r^2 \frac{\partial c_{\mathrm{s}}^{\pm}}{\partial r}(t,r)\right], \tag{28}$$

$$\frac{\partial c_{\mathrm{s}}^{\pm}}{\partial r}(t,0) = 0, \tag{29}$$

$$\frac{\partial c_{\mathrm{s}}^{+}}{\partial r}\left(t,R_{\mathrm{s}}^{+}\right) = \frac{1}{D_{\mathrm{s}}^{+} F a_{\mathrm{s}}^{+} L^{+}} I(t), \tag{30}$$

$$\frac{\partial c_{\mathrm{s}}^{-}}{\partial r}\left(t,R_{\mathrm{s}}^{-}\right) = -\frac{1}{D_{\mathrm{s}}^{-} F a_{\mathrm{s}}^{-} L^{-}} I(t) + \frac{(1-t_c^0)\, a_{\mathrm{s}}^{-}}{\varepsilon_{\mathrm{e}}^{-}} \bar{j}_{SR}^{-}(t), \tag{31}$$

where $\bar{j}_{SR}^{-}(t)$ is the average side-reaction current density over the negative electrode domain. The electrolyte-phase lithium concentration dynamics for the SPMe are given by:

$$\frac{\partial c_{\mathrm{e}}^{+}}{\partial t}(t,x) = \frac{D_{\mathrm{e}}^{+,\mathrm{eff}}(c_{\mathrm{e}}^{+}(t,x))}{\varepsilon_{\mathrm{e}}^{+}}\frac{\partial^2 c_{\mathrm{e}}^{+}}{\partial x^2}(t,x) - \frac{(1-t_{\mathrm{c}}^{0})}{\varepsilon_{\mathrm{e}}^{+} F L^{+}} I(t), \tag{32}$$

$$\frac{\partial c_{\mathrm{e}}^{-}}{\partial t}(t,x) = \frac{D_{\mathrm{e}}^{-,\mathrm{eff}}(c_{\mathrm{e}}^{-}(t,x))}{\varepsilon_{\mathrm{e}}^{-}}\frac{\partial^2 c_{\mathrm{e}}^{-}}{\partial x^2}(t,x) + \frac{(1-t_{\mathrm{c}}^{0})}{\varepsilon_{\mathrm{e}}^{-} F L^{-}} I(t) + \frac{(1-t_c^0)\, a_{\mathrm{s}}^{-}}{\varepsilon_{\mathrm{e}}^{-}} j_{\mathrm{SR}}^{-}(t,x), \tag{33}$$

$$\frac{\partial c_{\mathrm{e}}^{\mathrm{sep}}}{\partial t}(t,x) = \frac{\partial}{\partial x}\left[\frac{D_{\mathrm{e}}^{\mathrm{sep,eff}}(c_{\mathrm{e}}^{\mathrm{sep}}(t,x))}{\varepsilon_{\mathrm{e}}^{\mathrm{sep}}}\frac{\partial c_{\mathrm{e}}^{\mathrm{sep}}}{\partial x}(t,x)\right]. \tag{34}$$

The boundary conditions for the electrolyte lithium concentration PDEs in (32)–(34) are consistent with those of the DFN model given in (18)–(21). In the SPMe+SR model, the solid-phase potential is spatially uniform and depends on time only, consistent with standard SPMe asymptotics [10]. The electrolyte potential $\phi_e^{-}(t,x)$ is obtained from (7). These potentials are required in Section III to construct the reformulated models.

III. Models of Side-Reaction Mechanisms

In this section, reformulated models for SEI growth and lithium plating are proposed. The models assume a separation-of-variables structure that simplifies analysis and reduces computational cost while retaining key dynamics for fault diagnosis.

A. Reformulated model of SEI film growth

The reformulated SEI fault term provides a low-cost parameterization of the reference SEI model in (13) and is defined as [4]:

$$f_{\mathrm{SEI}}^{-}(t,x) = \theta_{\mathrm{SEI}}\Omega_{\mathrm{SEI}}(t-t_{\mathrm{fau}})\beta_{\mathrm{SEI}}(x)c_{\mathrm{e}}^{-}(t,L^{-}). \tag{35}$$

In the following, each term of the proposed fault model (35) is detailed below and linked to the SEI fault in (13). The SPMe asymptotics approximation assumes that the solid-phase potential is spatially uniform to leading order, i.e., $\phi_{\mathrm{s}}^{-}(t,x) \approx \phi_{\mathrm{s}}^{-}(t)$ [3]. Substituting this into (13) gives

$$j_{\mathrm{SEI}}^{-}(t,x) = -\frac{1}{F} i_{0,\mathrm{SEI}}^{-} \exp\Big(-\alpha_{\mathrm{SEI}}\frac{F}{RT}(\phi_{\mathrm{s}}^{-}(t) - U_{\mathrm{SEI}}^{-}(t) - \frac{R_f^{-}(t)}{a_{\mathrm{s}}^{-} L^{-}} I(t) - \phi_{\mathrm{e}}^{-}(t,x))\Big). \tag{36}$$

Define

$$A_{\mathrm{s}}(t) \triangleq \phi_{\mathrm{s}}^{-}(t) - U_{\mathrm{SEI}}(t) - \frac{R_f^{-}(t)}{a_{\mathrm{s}}^{-} L^{-}} I(t), \gamma_{\mathrm{s}} \triangleq \frac{\alpha_{\mathrm{SEI}} F}{RT}, \tag{37}$$

then, substituting (37) in (36), one obtains

$$j_{\mathrm{SEI}}^{-}(t,x) = -\frac{1}{F} i_{0,\mathrm{SEI}}^{-} \exp\left(-\gamma_{\mathrm{s}}(A_{\mathrm{s}}(t) - \phi_e^{-}(t,x))\right). \tag{38}$$

Now we focus on the electrolyte potential term $\phi_{\mathrm{e}}^{-}(t,x)$. For simplicity, we make the following assumption:

Authorized licensed use limited to: Texas Tech University. Downloaded on September 03,2026 at 21:39:47 UTC from IEEE Xplore. Restrictions apply.

Assumption 1. *The effective electrolyte conductivity, $\kappa_e^{-,\text{eff}}(c_e^-(t,x))$, is assumed to be constant.*

Based on Assumption 1 and the dilute-solution approximation, under which variations in the activity coefficient are neglected [11, Chapter 11], the thermodynamic factor $\left(1+\frac{d\ln f_{c/a}}{d\ln c_e^-}\right)$ is approximated as unity. The electrolyte potential (7) in the negative electrode for the SPMe simplifies to

$$\frac{\partial \phi_{\text{e}}^-}{\partial x}(t,x)=\frac{-i_{\text{e}}^-(t)}{\kappa_{\text{e}}^{-,\text{eff}}}+\frac{2RT}{F}\left(1-t_c^0\right)\frac{\partial \ln c_{\text{e}}^-}{\partial x}(t,x). \quad (39)$$

Taking the integral of (39), one obtains

$$\phi_{\text{e}}^-(t,x)=-\frac{i_{\text{e}}^-(t)}{\kappa_{\text{e}}^{-,\text{eff}}}\,x+\frac{2RT}{F}\left(1-t_c^0\right)\ln c_{\text{e}}^-(t,x)+Z_{\text{s}}(t), \quad (40)$$

where $Z_{\text{s}}(t)=\frac{2RT}{F}\left(1-t_c^0\right)\ln c_{\text{e}}^-(t,0^-)$ denotes the integration constant determined from the boundary condition (22). By substituting (40) into (38), one obtains

$$j_{\text{SEI}}^-(t,x)=-\frac{1}{F}i_{0,\text{SEI}}^-\exp\left(-\gamma_{\text{s}}A_{\text{s}}(t)\right)\times \exp\left(\gamma_{\text{s}}\left(-\frac{i_{\text{e}}^-(t)}{\kappa_{\text{e}}^{-,\text{eff}}}x+\frac{2RT}{F}\left(1-t_c^0\right)\ln c_{\text{e}}^-(t,x)+Z_{\text{s}}(t)\right)\right). \quad (41)$$

To proceed from (41) to the reformulated model (35), the following assumption is introduced:

Assumption 2 (Piecewise-constant electrolyte current over short windows)**.** *Over each estimation window $[t_0,\, t_0+\Delta t]$, the electrolyte current density $i_{\text{e}}(t)$ is approximated by a constant value, i.e., $i_{\text{e}}^-(t)\approx i_{\text{e}}^-$ for $t\in[t_0,\, t_0+\Delta t]$.*

This assumption is justified by noting that, even under dynamic load profiles such as Urban Dynamometer Driving Schedule (UDDS) [9], the current can be regarded as piecewise constant when viewed over sufficiently short windows. In practice, the window length Δt is chosen small enough so that the relative variation of $i_{\text{e}}^-(t)$ within the window remains negligible compared to its mean level. Under Assumption 2, for all $t\in[t_0,t_0+\Delta t]$ and $x\in[0^-,L^-]$, (41) simplifies to:

$$j_{\text{SEI}}^-(t,x)=-\frac{1}{F}i_{0,\text{SEI}}^-\exp\left(-\gamma_{\text{s}}\left(A_{\text{s}}(t)-Z_{\text{s}}(t)\right)\right) \exp\left(\gamma_{\text{s}}\left(-\frac{i_{\text{e}}}{\kappa_0}x\right)\right)c_{\text{e}}^-(t,x)^{2\alpha_{\text{SEI}}\left(1-t_c^0\right)}. \quad (42)$$

In the following, the mapping of each term of the reformulated model in (35) to the reference model in (42) is discussed.

- **Fault intensity (θ_{SEI}):** In the reformulated model (35), the coefficient θ_{SEI} represents the SEI fault magnitude (fault intensity) and corresponds to $\frac{1}{F}i_{0,\text{SEI}}^-$ in (42).
- **Fault time profile term $\Omega_{\text{SEI}}(t-t_{\text{fau}})$:** $A_{\text{s}}(t)$ in (42) denotes the SEI effective overpotential. The factor $\exp[-\gamma_{\text{s}}(A_{\text{s}}(t)-Z_{\text{s}}(t))]$ in (42) captures the time-dependency of the SEI side reaction. Since SEI film growth increases the film resistance $R_f^{\pm}(t)$, $A_{\text{s}}(t)$ decreases, which in turn reduces the SEI reaction. Thus, $A_{\text{s}}(t)-Z_{\text{s}}(t)$ decreases after fault initiation, and $\exp[-\gamma_{\text{s}}(A_{\text{s}}(t)-Z_{\text{s}}(t))]$ shows a saturating behavior. It rises initially, then slows, and finally converges to an upper bound of unity. For simplification and to reduce computational complexity, the temporal evolution of the SEI fault is approximated by the function $\Omega_{\text{SEI}}(t)$ which is a limited-resource population growth model [12] as follows:

$$\Omega_{\text{SEI}}(t)=\begin{cases}0, & t<t_{\text{fau}},\\ 1-e^{-a_{\text{SEI}}(t-t_{\text{fau}})}, & t\geq t_{\text{fau}},\end{cases} \quad (43)$$

  t_{fau} denotes the time at which the side-reaction magnitude deviates from its nominal behavior and a_{SEI} is a positive constant inspired by population growth models.
- **Spatial fault growth rate ($\beta_{\text{SEI}}(x)$):** In (42), the spatial dependence of the SEI fault term appears as $\exp\left[\gamma\left(-\frac{i_{\text{e}}^-}{\kappa_{\text{e}}^{-,\text{eff}}}x\right)\right]$. Under typical discharge conditions ($i_{\text{e}}^-<0$ in the negative electrode), the exponential factor increases with x and reaches its maximum at the electrode–separator interface ($x=L^-$). Since the electrode thickness $x\in\{0,L^-\}$ is small, the term $\frac{i_{\text{e}}^-}{\kappa_{\text{e}}^{-,\text{eff}}}x$ remains small over the spatial domain. In this range, the exponential can be approximated by its first-order Taylor expansion,

$$\exp\left[\gamma\left(-\frac{i_{\text{e}}^-}{\kappa_{\text{e}}^{-,\text{eff}}}x\right)\right]\approx 1+\gamma\left(-\frac{i_{\text{e}}^-}{\kappa_{\text{e}}^{-,\text{eff}}}\right)x, \quad (44)$$

  which is linear in x. Experimental evidence indicates that SEI film growth is more pronounced near the separator, (see [13, Fig. 13]). The growth rate at the negative electrode/separator interface is more pronounced than in other regions of the negative electrode [13]. Consider the following assumption for spatial term modeling:

  Assumption 3 (Fault growth rate)**.** *According to the spatial distribution of the SEI layer illustrated in [13, Fig. 13], the SEI film growth rate shows a mild gradient across the negative electrode. Thus it is assumed to be proportional to the spatial coordinate:*

$$\beta_{SEI}(x)\triangleq\beta_{SEI,0^-}+\frac{\beta_{SEI,L^-}-\beta_{SEI,0^-}}{L^-}x, \quad (45)$$

  where $\beta_{SEI,0^-}=\beta_{SEI}(0^-)$ represents the SEI film growth rates at the negative current collector boundary and $\beta_{SEI,L^-}=\beta_{SEI}(L^-)$ denotes the SEI film growth rates at the negative electrode–separator interface.

  The reformulated model adopts a linear form consistent with (44). Therefore, $\beta_{\text{SEI}}(x)$ can be interpreted as the linearized approximation of the exponential spatial dependence in the reference model.
- **Lithium concentration effect:** In (42), the electrolyte concentration appears as $c_{\text{e}}^-(t,x)^{2\alpha_{\text{SEI}}(1-t_c^0)}$. For the parameter values $\alpha_{\text{SEI}}=0.5$ and $t_c^0=0.22$ reported in [14], the exponent becomes 0.78, which approximates to unity indicating a linear dependence on $c_{\text{e}}^-(t,x)$. Because the concentration at this boundary has the strongest influence, in the reformulated model (35), this

Authorized licensed use limited to: Texas Tech University. Downloaded on September 03,2026 at 21:39:47 UTC from IEEE Xplore. Restrictions apply.

term is simplified to a linear dependence on the electrolyte concentration at the negative electrode–separator boundary, $c_{\mathrm{e}}^{-}(t, L^{-})$. This captures the main effect of the boundary electrolyte concentration in accelerating the SEI side reaction, while maintaining a lower model complexity.

B. Reformulated model of lithium plating

The reformulated lithium plating fault model is defined as:

$$f_{\mathrm{pl}}^{-}(t,x) = \theta_{\mathrm{pl}}\Omega_{\mathrm{pl}}(t - t_{\mathrm{fau}})\beta_{\mathrm{pl}}(x)c_{\mathrm{e}}^{-}(t, L^{-}). \tag{46}$$

In the following, each term of the proposed model is explained in detail. By applying the spatial uniformity of solid-phase electric potential in (14), it can be rewritten as:

$$j_{\mathrm{pl}}^{-}(t,x) = -\frac{1}{F}i_{0,\mathrm{pl}}^{-}\exp\big(-\alpha_{\mathrm{pl}}\tfrac{F}{RT}(\phi_{\mathrm{s}}^{-}(t) - U_{\mathrm{pl}}^{-}(t) - \tfrac{R_f^{-}(t)}{a_{\mathrm{s}}^{-}L^{-}}I(t) - \phi_{\mathrm{e}}^{-}(t,x))\big). \tag{47}$$

Lithium plating occurs when the plating overpotential satisfies $\eta_{pl}(t,x) < 0$. This electrochemical onset condition is inherently respected in the present formulation, since the model is derived from the detailed electrochemical kinetics. Define

$$A_{\mathrm{p}}(t) \triangleq \phi_{\mathrm{s}}^{-}(t) - U_{\mathrm{pl}}(t) - \frac{R_f^{-}(t)}{a_{\mathrm{s}}^{-}L^{-}}I(t), \gamma_{\mathrm{p}} \triangleq \frac{\alpha_{\mathrm{pl}}F}{RT}. \tag{48}$$

Substituting definitions in (48) into (47) yields

$$j_{\mathrm{pl}}^{-}(t,x) = -\frac{1}{F}i_{0,\mathrm{pl}}^{-}\exp\left(\gamma_{\mathrm{p}}\left(\phi_{\mathrm{e}}^{-}(t,x) - A_{\mathrm{p}}(t)\right)\right). \tag{49}$$

Employing (40) and under Assumption 1 and 2, equation (49) is written as:

$$j_{\mathrm{pl}}^{-}(t,x) = -\frac{1}{F}i_{0,\mathrm{pl}}^{-}\exp\left(-\gamma_{\mathrm{p}}\left(A_{\mathrm{p}}(t) - Z_{\mathrm{p}}(t)\right)\right) \exp\left(\gamma_{\mathrm{p}}\left(-\frac{i_{\mathrm{e}}}{\kappa_{\mathrm{e}}^{-,\mathrm{eff}}}x\right)\right)c_{\mathrm{e}}^{-}(t,x)^{2\alpha_{\mathrm{pl}}(1-t_c^0)}. \tag{50}$$

Next, each term of the reformulated plating fault in (46) will be mapped to the corresponding term in (50). This mapping clarifies the preserved physics and the simplified mathematical representation.

- **Fault intensity (θ_{pl}):** In the reformulated model, θ_{pl} denotes the magnitude of the fault effect expressing the fault intensity. This matches the factor $\frac{1}{F}i_{0,\mathrm{pl}}^{-}$ in (50).
- **Fault time profile term $\Omega_{\mathrm{pl}}(t - t_{\mathrm{fau}})$:** The exponential factor $\exp[-\gamma_{\mathrm{p}}(A_{\mathrm{p}}(t) - Z_{\mathrm{p}}(t))]$ represents the time-dependent term of the lithium plating side reaction. When lithium plating occurs, as indicated in the structure, $A_{\mathrm{p}}(t) - Z_{\mathrm{p}}(t)$ decreases after fault initiation. Consequently, $\exp[-\gamma_{\mathrm{p}}(A_{\mathrm{p}}(t) - Z_{\mathrm{p}}(t))]$ exhibits a saturating behavior, which is described by a limited-resource population growth model, as follows:

$$\Omega_{\mathrm{pl}}(t) = \begin{cases} 0, & t < t_{\mathrm{fau}}, \\ 1 - e^{-a_{\mathrm{pl}}(t - t_{\mathrm{fau}})}, & t \geq t_{\mathrm{fau}}, \end{cases} \tag{51}$$

where a_{pl} is a positive constant which controls the speed of growth of the plating fault time profile.

Remark 2. *In the fault time profiles,* (43) *and* (51)*, $a_{\mathrm{pl}} \gg a_{\mathrm{SEI}}$, because SEI film growth leads to gradual capacity loss [15], whereas lithium plating initiates abruptly under fast-charging or low-temperature conditions, resulting in a much steeper temporal rise.*

- **Spatial fault growth rate ($\beta_{\mathrm{pl}}(x)$):** Lithium plating is localized at the separator-negative electrode boundary, and thus modeled with a sharp profile:

$$\beta_{\mathrm{pl}}(x) = e^{a_{\mathrm{pl}}x/L^{-}}, \tag{52}$$

In the reference model (50), the exponential dependence on x indicates stronger plating near the separator. The reformulated model replaces this with the simpler form as (52). It captures the essential behavior: low at the terminal boundary and rapidly increasing toward separator boundary, $x = L^{-}$.

- **Lithium concentration effect:** In (50) there is dependence on electrolyte concentration. To represent this effect, linear dependence on $c_{\mathrm{e}}^{-}(t, L^{-})$ is added to the reformulated fault model (46) because lithium plating is more localized on the separator boundary ($x = L^{-}$). This reflects the primary influence of the boundary electrolyte concentration on accelerating the lithium plating side reaction, while preserving a simpler model.

IV. Simulation

The proposed reformulated models for SEI and lithium plating electrochemical faults are simulated for a $LiFePO_4$ cell with the parameters referenced from Table 1 in [14]. The system input, given by the UDDS current profile [9], is depicted in Fig. 3. The SEI reformulated model function for

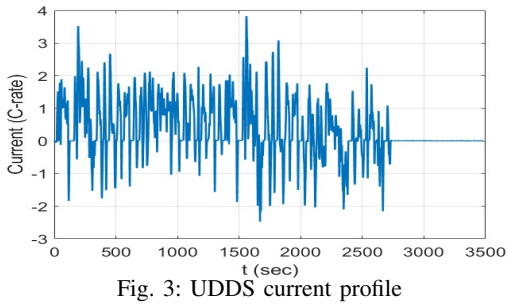

Fig. 3: UDDS current profile

the simulation is defined as follows:

$$f_{\mathrm{SEI}}^{-}(t,x) = 50(1 - e^{-0.0001(t-1000)})c_{\mathrm{e}}^{-}(t, L^{-}) \times \left(\beta_{\mathrm{SEI}}(0^{-}) + \left(\beta_{\mathrm{SEI}}(L^{-}) - \beta_{\mathrm{SEI}}(0^{-})\right)x\right), \tag{53}$$

where $\beta_{\mathrm{SEI}}(0^{-}) = 31 \times 10^{-13}$ and $\beta_{\mathrm{SEI}}(L^{-}) = 36 \times 10^{-13}$ [13]. At $t_{\mathrm{fau}} = 1000\,\mathrm{s}$, the lithium plating side reaction becomes active. This is illustrated in Fig. 4. As t increases, the second term approaches 1. The contribution of the last term remains negligible due to the slow evolution and small thickness of the SEI layer. Consequently, the fault is primarily dominated by $c_{\mathrm{e}}^{-}(t, L^{-})$. This dominant influence can be observed in Fig. 4, where, after the fault occurs at

Authorized licensed use limited to: Texas Tech University. Downloaded on September 03,2026 at 21:39:47 UTC from IEEE Xplore. Restrictions apply.

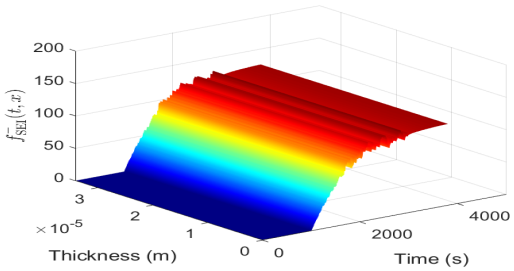

Fig. 4: Distributed SEI fault $f_{\text{SEI}}^{-}(t,x)$.

$t_{\text{fau}} \geq 1000\,\text{s}$, the fault trajectory closely follows the system state. The reformulated plating fault function for simulation, based on the model in (46), is defined as follows:

$$f_{\text{pl}}^{-}(t,x) = 50(1-e^{-0.01(t-1000)})e^{0.01x}c_{\text{e}}^{-}(t,L^{-}), \quad (54)$$

Fig. 5 depicts the distributed plating activated at $t_{\text{fau}} = 1000\,\text{s}$. In Figs. 4 and 5, both reformulated fault profiles

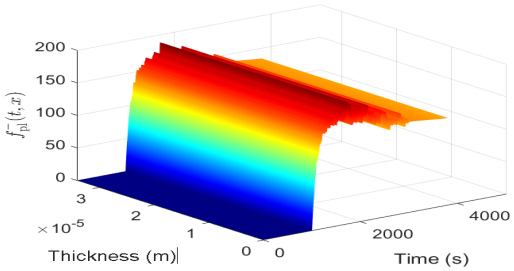

Fig. 5: Distributed plating fault $f_{\text{pl}}^{-}(t,x)$.

exhibit negligible x-direction variation due to small electrode thickness and low C-rate, which keep electrolyte concentration nearly uniform and spatial gradients weak. Fig. 6 illustrates the comparison between the reformulated plating and SEI faults at the electrode boundary $x = L^{-}$. The results confirm that the SEI fault evolves more gradually compared to the plating fault. This behavior directly reflects the values of the growth parameters: $a_{\text{SEI}} = 0.0001$ and $a_{\text{pl}} = 0.1$. The SEI fault grows steadily, whereas the plating fault reaches higher magnitudes earlier, consistent with $a_{\text{pl}} \gg a_{\text{SEI}}$ (Remark 2).

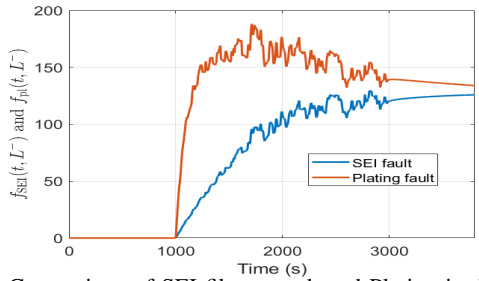

Fig. 6: Comparison of SEI film growth and Plating in the negative electrode.

V. Conclusion and Future Work

To overcome the complexity of the DFN+SR model with SEI film growth and lithium plating, reformulated side-reaction models are derived in the SPMe+SR framework for these mechanisms. The reformulation preserves physical consistency while reducing computational cost. The behavior of these models is illustrated through simulations on a $LiFePO_4$ cell. As part of future work, the proposed reformulated fault model will be validated in comparison with the DFN+SR model to further confirm its accuracy and physical consistency. The modeling framework can also be extended to incorporate additional degradation mechanisms, such as lithium loss due to active material isolation and electrode cracking, and thermal effects that strongly influence fault dynamics will be considered as well.

References

[1] Pallavi Verma, Pascal Maire, and Petr Novák. A review of the features and analyses of the solid electrolyte interphase in li-ion batteries. *Electrochimica Acta*, 55(22):6332–6341, 2010.

[2] Jacqueline S Edge, Simon O'Kane, Ryan Prosser, Niall D Kirkaldy, Anisha N Patel, Alastair Hales, Abir Ghosh, Weilong Ai, Jingyi Chen, Jiang Yang, et al. Lithium ion battery degradation: what you need to know. *Physical Chemistry Chemical Physics*, 23(14):8200–8221, 2021.

[3] Ferran Brosa Planella and W Dhammika Widanage. A single particle model with electrolyte and side reactions for degradation of lithium-ion batteries. *Applied Mathematical Modelling*, 121:586–610, 2023.

[4] Sara Sepasiahooyi and Shu-Xia Tang. Fault diagnosis of electrolyte lithium concentration in lithium-ion batteries. In *Proceedings of the 2025 American Control Conference (ACC)*. IEEE, 2025.

[5] Nalin A Chaturvedi, Reinhardt Klein, Jake Christensen, Jasim Ahmed, and Aleksandar Kojic. Algorithms for advanced battery-management systems. *IEEE Control systems magazine*, 30(3):49–68, 2010.

[6] Xiao-Guang Yang, Yongjun Leng, Guangsheng Zhang, Shanhai Ge, and Chao-Yang Wang. Modeling of lithium plating induced aging of lithium-ion batteries: Transition from linear to nonlinear aging. *Journal of Power Sources*, 360:28–40, 2017.

[7] Aiping Wang, Sanket Kadam, Hong Li, Siqi Shi, and Yue Qi. Review on modeling of the anode solid electrolyte interphase (SEI) for lithium-ion batteries. *NPJ Computational materials*, 4(1):15, 2018.

[8] Xuekun Lu, Marco Lagnoni, Antonio Bertei, Supratim Das, Rhodri E Owen, Qi Li, Kieran O'Regan, Aaron Wade, Donal P Finegan, Emma Kendrick, et al. Multiscale dynamics of charging and plating in graphite electrodes coupling operando microscopy and phase-field modelling. *Nature Communications*, 14(1):5127, 2023.

[9] Scott J Moura, Federico Bribiesca Argomedo, Reinhardt Klein, Anahita Mirtabatabaei, and Miroslav Krstic. Battery state estimation for a single particle model with electrolyte dynamics. *IEEE Transactions on Control Systems Technology*, 25(2):453–468, 2016.

[10] Saeed Khaleghi Rahimian, Sean Rayman, and Ralph E White. Extension of physics-based single particle model for higher charge–discharge rates. *Journal of Power Sources*, 224:180–194, 2013.

[11] John Newman and Nitash P Balsara. *Electrochemical systems*. John Wiley & Sons, 2021.

[12] Basel M Al-Eideh and Hana O Al-Omar. Population projection model using exponential growth function with a birth and death diffusion growth rate processes. *Eur. J. Sci. Res*, 151(3):271–276, 2019.

[13] Lin Liu, Jonghyun Park, Xianke Lin, Ann Marie Sastry, and Wei Lu. A thermal-electrochemical model that gives spatial-dependent growth of solid electrolyte interphase in a li-ion battery. *Journal of power sources*, 268:482–490, 2014.

[14] Clément Edouard, Martin Petit, C Forgez, Julien Bernard, and Renaud Revel. Parameter sensitivity analysis of a simplified electrochemical and thermal model for Li-ion batteries aging. *Journal of Power Sources*, 325:482–494, 2016.

[15] Serena Carelli and Wolfgang G Bessler. Coupling lithium plating with SEI formation in a pseudo-3D model: A comprehensive approach to describe aging in lithium-ion cells. *Journal of The Electrochemical Society*, 169(5):050539, 2022.

Authorized licensed use limited to: Texas Tech University. Downloaded on September 03,2026 at 21:39:47 UTC from IEEE Xplore. Restrictions apply.